

# 3D simulation of a power ramp including oxygen thermo-diffusion and its impact on thermochemistry

P. Konarski, J. Sercombe, C. Riglet-Martial, I. Zacharie-Aubrun, M. Fregonese, P. Chantrenne

▶ **To cite this version:**

P. Konarski, J. Sercombe, C. Riglet-Martial, I. Zacharie-Aubrun, M. Fregonese, et al.. 3D simulation of a power ramp including oxygen thermo-diffusion and its impact on thermochemistry. TOPFUEL 2018 - Light Water Reactor (LWR) Fuel Performance Meeting, Sep 2018, Prague, Czech Republic. cea-02400207

**HAL Id: cea-02400207**
**https://cea.hal.science/cea-02400207**

Submitted on 21 Feb 2020

**HAL** is a multi-disciplinary open access archive for the deposit and dissemination of scientific research documents, whether they are published or not. The documents may come from teaching and research institutions in France or abroad, or from public or private research centers.

L'archive ouverte pluridisciplinaire **HAL**, est destinée au dépôt et à la diffusion de documents scientifiques de niveau recherche, publiés ou non, émanant des établissements d'enseignement et de recherche français ou étrangers, des laboratoires publics ou privés.

# 3D SIMULATION OF A POWER RAMP INCLUDING OXYGEN THERMO-DIFFUSION AND ITS IMPACT ON THERMOCHEMISTRY

P. KONARSKI, J. SERCOMBE, CH. RIGLET-MARTIAL, I. ZACHARIE-AUBRUN
*CEA, DEN, DEC*
*13108 Saint-Paul lez Durance – France*

M. FRÉGONÈSE, P. CHANTRENNE
*MATEIS UMR 5510, INSA-Lyon*
*69621 Villeurbanne - France*

## ABSTRACT

This paper presents the coupling of the thermochemical solver ANGE (Advanced Gibbs Energy Minimizer) with an oxygen thermo-diffusion model. The coupling is implemented within the fuel performance code ALCYONE co-developed by CEA, EDF and FRAMATOME within the PLEIADES environment. An application to a 3D simulation of a power ramp on a Cr-doped $UO_2$ fuel is developed. Post-ramp EPMA measurements of chromia doped fuel show reduction of chromium and molybdenum oxides in the central part of the pellet, indicative of thermo-diffusion of oxygen. These phenomena are well reproduced by the coupled thermo-chemical-mechanical simulations.
Impact of oxygen redistribution on speciation of fission products is then studied. Chemical state of caesium, iodine and tellurium is important as regard PCI, as they can form gaseous species ($CsI_{(g)}$, $I_{(g)}$, $I_{2(g)}$, $TeI_{2(g)}$) that can react with the cladding and induce SCC. Release of gaseous species and concentration of chemically reactive iodine compounds near the cladding are calculated in order to investigate I-SCC.

## 1. Introduction

During irradiation, the composition and the structure of the fuel vary. Numerous fission products and actinides create together a very complex chemical system. This system is separated from the surroundings by the cladding. The integrity of the cladding ensures the confinement of the fission products in the fuel rod. However, Pellet-Cladding Interaction (PCI) induced by fuel cracking, swelling and the non uniform axial pellet deformation combined with the release of chemically reactive fission gases from the fuel pellet centre can lead to Iodine Stress Corrosion Cracking (I-SCC) of the cladding.
Coupling of thermo-chemical and thermo-mechanical codes allow to investigate both chemical and mechanical factors simultaneously [1]. It is in particular important to understand the behaviour of dopants in fuels that have shown an improved resistance to PCI failure [2]. In a recent paper on power ramped Cr-doped fuels [3], it has been shown that the oxygen potential along the fuel radius strongly varies during the high power period of the power ramp, which is indicative of oxygen thermo-diffusion induced by the high thermal gradient in the fuel. The oxygen potential variations affect the chemical speciation of the fission products in the fuel and should therefore be considered in PCI simulations.
In this paper, we present 3D thermo-chemical-mechanical simulations of power ramps on Cr-doped $UO_2$ with the fuel performance code ALCYONE including thermo-diffusion of oxygen. The main purpose of our latter development is to study the impact of oxygen redistribution on fission products thermo-chemistry and on corrosive Fission Gas Release. A new method has been developed in this work to couple oxygen thermo-diffusion and FP thermo-chemistry. It ensures fast calculations which make 3D simulations possible and guaranties the simultaneous conservation of oxygen atoms and vacancies in the pellet.
Part 2 describes the fuel performance code ALCYONE and the main models used in the coupled simulation. Part 3 details the modelling of oxygen thermo-diffusion. Simulation results are shown and discussed in part 4.

## 2. The fuel performance code ALCYONE

ALCYONE is a multidimensional fuel performance code part of the PLEIADES environment co-financed by EDF and FRAMATOME. ALCYONE is able to perform simulations of the fuel rod behaviour in nominal conditions, power ramps and accidental conditions [4]. It is possible to simulate different geometries. The most basic one stems from the 1.5D scheme where the fuel rod is divided into axial slices and then slices into concentric rings. Quantities calculated include temperature, fuel and cladding displacements, fission gas release and stresses. These quantities are also calculated by the 2D and 3D schemes which simulate the behaviour of a fuel pellet fragment. In 2D, the mid-pellet plane of a fuel pellet fragment is considered while in 3D one quarter of a fuel pellet fragment is meshed with the cladding. Thermo-mechanical calculations in the three configurations rely on the finite element code Cast3M [5]. Examples of discretisation in 2D and 3D are shown in Fig. 1.

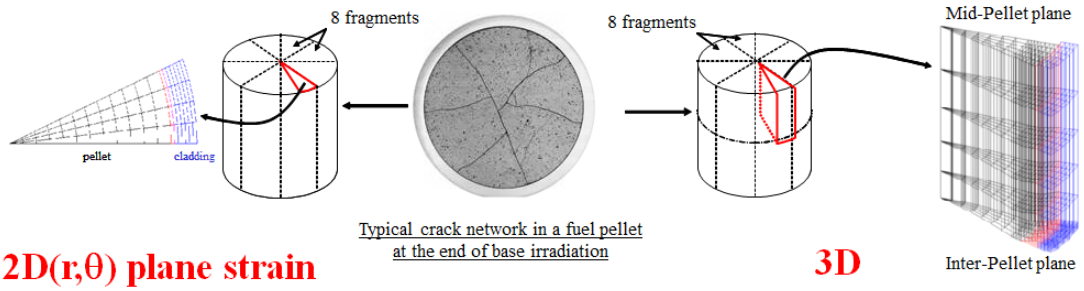



Fig. 1 Examples of meshes in 2D and 3D. A fuel pellet is divided in 8 fragments in order to account for the crack network that forms during nominal irradiation.

### 2.1. The depletion code CESAR

The quantities of FPs used in the simulations are based on calculations performed with the code CESAR [6]. CESAR estimates the depletion, decay and transmutation of isotopes. In order to accelerate calculations, a set of empirical linear correlations describing evolution of FP concentrations with the fuel burnup has been derived [2]. These correlations are valid up to 100 GWd/tU. Additionally, some FPs have similar chemical behaviour. Thus it is possible to represent a group FPs with only one of them. Elements taken into account, their affiliations to families and quantities per mol of $UO_2$ and GWd/tU are given in Tab. 1.

| Elements | Representative Element | Creation (mol / mol $UO_2$ / GWd / tU) | Family |
|---|---|---|---|
| Xe + Kr | Xe | 3.36E-04 | Inert fission gas and volatile fission products |
| Cs + Rb | Cs | 1.87E-04 | |
| I + Br | I | 3.32E-05 | |
| Te + Se | Te | 1.44E-05 | |
| Ba + Sr | Ba | 2.58E-04 | Stable oxides |
| Zr + Nb | Zr | 1.52E-04 | |
| Mo | Mo | 2.88E-04 | |
| Ru + Tc + Rh | Ru | 1.36E-04 | Metallic fission products |
| Pd | Pd | 1.02E-04 | |
| Ce | Ce | 2.11E-04 | Fission products in solid solution in $UO_2$ |
| Eu + Sm | Eu | 4.19E-05 | |
| La + Y | La | 2.69E-04 | |
| Gd + Nd + Pm | Gd | 1.12E-04 | |
| Pu + Pr | Pu | 3.70E-04 | |

Tab. 1 Quantities of fission products per mol of initial $UO_2$ and GWd/tU [2].

In addition, the decrease of the U content of the fuel with fission is taken into account. An example of calculation performed with the empirical correlations from Tab. 1 is shown in

Fig. 2. The radial profile of burnup in the fuel is calculated by ALCYONE. Radial profiles of FPs are in good agreement with experimental measurements.

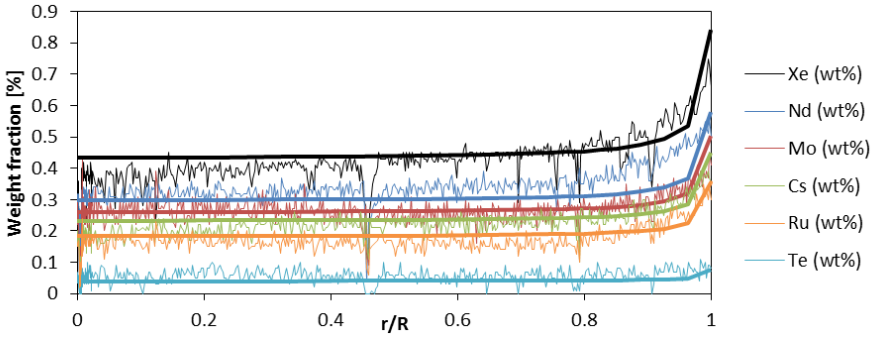



Fig. 2. Comparison of calculated weight fractions of FPs (thick lines) with EPMA measurements (thin lines) after the PR2 test (see Tab. 2).

### 2.2. The thermo-chemical solver ANGE

ANGE is a thermo-chemical solver based on the SOLGAMIX code [7]. It uses the Gibbs energy minimization method to find the thermodynamic equilibrium of the multicomponent and multiphase system at given temperature and pressure. ANGE uses a thermodynamic database that includes compounds occurring in different phases: the solid solution phase, the gas phase, stoichiometric separate phases and the noble metals phase.

- The fluorite oxide solid solution includes U, Pu and fission products (mostly rare earths). The thermodynamic description of the U-Pu-O system is based on the work of Lindemer and Besmann [8] [9]. The thermodynamic representation of rare earths comes from Lindemer and Brynestad [10]. The data for Eu and Zr come from Dumas [11]. The solubility of Ba is based on the experiments of Fujino [12]. The solubility of Cr is based on the model proposed by Riglet-Martial [13]. The solid solution phase contains 20 species.
- The gas phase is composed of 61 species. It includes gases important for PCI such as $Cs_{(g)}$, $Cs_{2(g)}$, $CsI_{(g)}$, $Cs_2I_{2(g)}$, $I_{(g)}$, $I_{2(g)}$, $Te_{(g)}$, $Te_{2(g)}$, $Te_{3(g)}$, $Te_{5(g)}$, $TeI_{2(g)}$ and $Cs_2MoO_{4(g)}$.
- The stoichiometric separate phases include solid and liquid uranates, molybdates and zirconates, such as $Cs_2UO_{4(s)}$, $Cs_2MoO_{4(s,l)}$, $Cs_2ZrO_{3(s)}$, $BaZrO_{3(s)}$, and other important coumpounds like $MoO_{2(s)}$, $MoO_{3(s)}$, $CsI_{(s,l)}$, $Te_{(s,l)}$, $Cs_{(s,l)}$, $Cs_2Te_{(s,l)}$, $BaTe_{(s)}$. 79 stoichiometric separate phases are considered in the database.
- The noble metals phase includes 3 species that are often observed simultaneously in irradiated fuels: $Mo_{(s)}$, $Ru_{(s)}$ and $Pd_{(s)}$.

The outputs of ANGE include the concentration of all the chemical species that are likely to appear, the ratio of oxygen to metal atoms in solid solution (O/M) and the oxygen potential. The oxygen potential characterizes the solid-gas equilibrium in the fuel is usually expressed by $\Delta G_{O_2} = R_g T \ln(p_{O_2}/p_{st})$ where $p_{O_2}$ is the oxygen partial pressure, $p_{st}$ is the standard pressure of 1 bar, $R_g$ is the ideal gas constant and $T$ is the temperature.

### 2.3. The fission gas release model CARACAS

CARACAS is a mechanistic model dealing with the inert fission gases – xenon and krypton. It can simulate the gas behaviour in various conditions including power transients, loss of coolant accidents and reactivity initiated accidents (LOCA, RIA). CARACAS distinguishes intra- and inter-granular gas populations. At high temperatures occurring during incidental and accidental conditions the fission gases created within the grain form intra-granular bubbles that migrate towards the grain face due to the thermal gradient. The gas contained in these bubbles can be re-dissolved within the grain by fission spikes. The gas reaching the grain face forms inter-granular bubbles. The next step is formation of inter-granular tunnels. When inter-granular bubbles cover more than 20% of the grain surface they gradually coalesce forming channels. When more than 10% of bubbles are coalesced the tunnels are assumed to be connected to the open porosity. FGR occurs when the pressure in these channels is greater that the plenum pressure. More details about the model can be found in the reference [14].

## 2.4. Modelling oxygen thermo-diffusion

Oxygen thermo diffusion is a well-known phenomenon occurring in Sodium Fast Reactors fuel. The equation describing solid-state thermo-diffusion of oxygen was formulated in the 1970's to explain the radial oxygen redistribution in initially non-stoichiometric but homogeneous $UO_{2+x}$ samples [15]. Oxygen thermo-diffusion describes the movement of oxygen point defects (interstitials or vacancies) under simultaneous temperature and concentration gradients. Instead of using the concentration of point defects, c $[\mathrm{mol\ mol\ UO_2}^{-1}]$, one may use alternatively the stoichiometry deviation, x $[-]$, or the oxygen over metal ratio, O/M $[-]$. The relation between them is as follows:

$$c = |x| = \left|\frac{O}{M} - 2\right|$$

The thermo-diffusion equation is given by [16]:

$$\frac{\partial x}{\partial t} = \vec{\nabla}\cdot\left[D\left(\vec{\nabla x} + \frac{xQ^*}{R_g T^2}\vec{\nabla T}\right)\right]$$

where $x$ is the stoichiometry deviation, $D\ [\mathrm{m^2\ s^{-1}}]$ is the oxygen chemical diffusion coefficient, $Q^*\ [\mathrm{J\ mol^{-1}}]$ stands for the heat of transport of oxygen, $R_g\ [\mathrm{J\ mol^{-1}}]$ is the gas constant and $T\ [\mathrm{K}]$ is the temperature. In non irradiated fuels, it has been shown experimentally that if the material is initially hyperstoichiometric $(x > 0)$, oxygen migrates up the temperature gradient (implying Q* > 0). If the material is initially hypostoichiometric $(x < 0)$, oxygen migrates to the cold part of the pellet, implying Q* < 0. The finite element code Cast3M is used in ALCYONE to solve the oxygen thermo-diffusion problem in 3D [5].

## 2.5. Coupling of the thermo-diffusion model with ALCYONE

Temperature, mechanical stresses and burnup at each node are calculated in the convergence loop of ALCYONE. The FGR model CARACAS and the thermochemical solver ANGE is added to this loop. ANGE uses the pre-ramp quantities of stable isotopes (calculated from burnup), temperature and pressure and calculates the chemical state of the system including the concentration of chemically reactive fission gases. Release of these gases is estimated in proportion to the release of rare gases and to the concentration of rare gases at inter-granular sites calculated by CARACAS. It is thus implicitly assumed that reactive fission gases are more easily released than rare gases, most of them being located in the inter-granular area. A schematic representation of the couplings is given in Fig. 3.

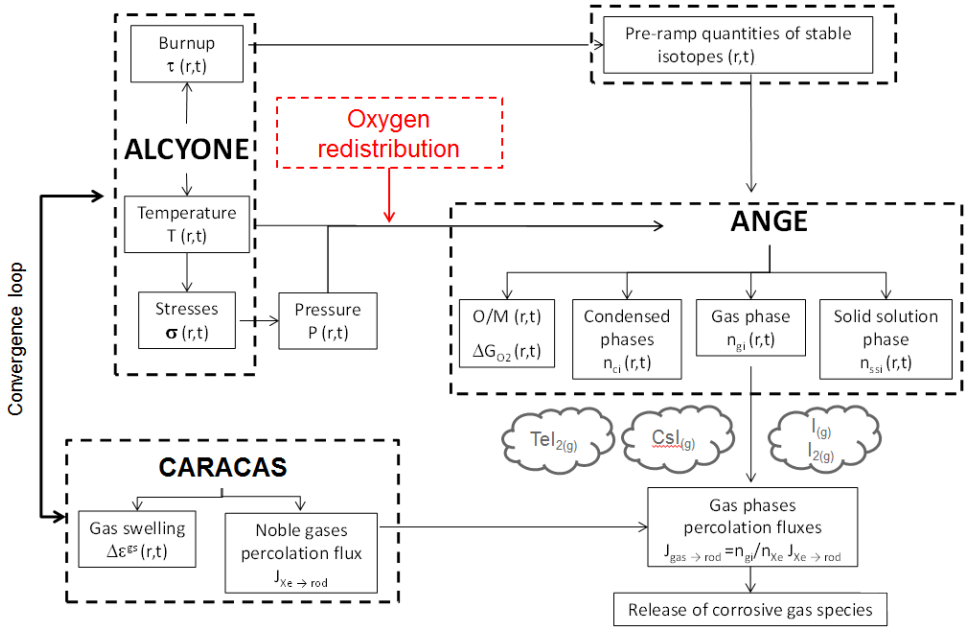



Fig. 3. Schematic representation of the coupling between the fuel performance code ALCYONE, the thermo-chemical solver ANGE, the fission gas release model CARACAS and the oxygen redistribution model.

The simulations described in this paper have been performed in ALCYONE 2.0 which is the newest version of the code, released in December 2016. It has several improvements compared to previous versions. For instance, several new models have been added in order to improve the modelling of incidental and accidental situations. The code optimisation has reduced computational times by more than 50% on average. One may find details of the new version and of its validation on an extensive database in reference [4].
Thermochemical computations during the power ramp are done with prescribed values of the O/M ratio and of the total oxygen concentration calculated by the oxygen redistribution model. A very steep evolution of the O/M ratio (see Fig. 7) causes convergence difficulties and requires adjusting the thermo-diffusion sub-time steps which are significantly smaller compared to global time steps.

## 3. 3D simulations of power ramps on Cr-doped fuels

To show the impact of oxygen redistribution on the thermo-chemical state of fission products, power ramp tests are simulated with ALCYONE. Details of the experiments are given in Tab. 2.

| Test name | $\%^{235}U$ | Dopant $Cr_2O_{3(ss)}$ (wt%) | Initial O/U | Average burnup (GWd/tU) | Max. LHR (W/cm) | Holding time (h) |
|---|---|---|---|---|---|---|
| PR1 | 4.9 | 0.16 | 2.00±0.01 | 38 | 470 | 12 |
| PR2 | 4.9 | 0.16 | 2.00±0.01 | 32 | 470 | 0 |

Tab. 2 Main characteristics of the ramp tests. PR1 is the main test simulated in this paper, PR2 is a similar power ramp but without a holding period.

The fuel rods underwent 3 irradiation cycles in a commercial PWR and then were used to fabricate rodlets for the ramp tests. The ramp tests start with a conditioning period. During this period, the sample recovers the thermo-mechanical conditions that it had during its last cycle in commercial PWR. At “t0 ramp” the power increases to reach its maximum at “t0 HP”. The Holding Period (HP) at the maximum Linear Heat Rate (LHR) lasts 12h and ends at “t0 HP +12h”. A schematic representation of the test is given in Fig. 4.

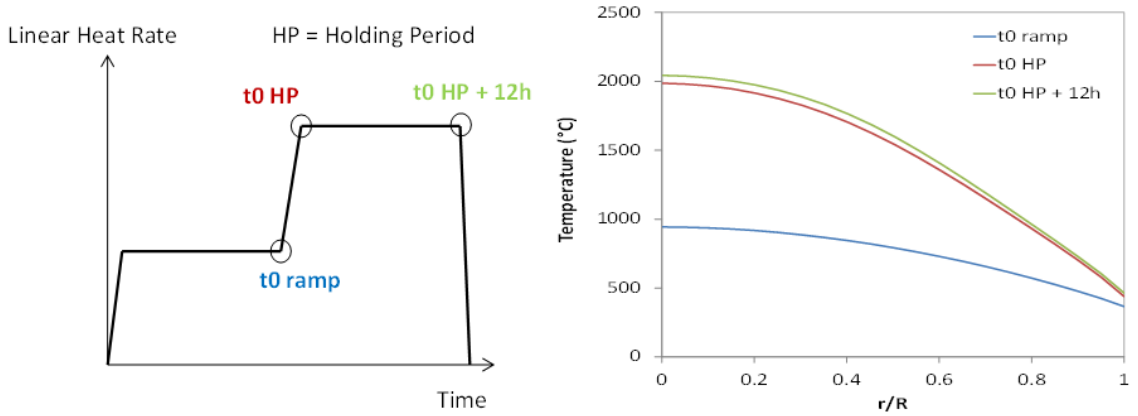



Fig. 4. Left figure: schematic representation of the simulated power ramp test. Right figure: radial temperature profiles at “t0 ramp”, “t0 HP” and at “t0 HP + 12h”.

The thermochemical and oxygen redistribution calculations shown in the following section are relative to the axial position of the maximum LHR of the rodlet and only concern the holding period (“t0 HP”→”t0 HP + 12h”) of the power ramp. In fact, it is assumed that the duration of the power transient “t0 ramp”→”t0 HP” is too short (~100 s) to lead to significant oxygen redistribution. Fig. 5 compares EPMA measurements of residual Cr weight fraction dissolved in the fuels after tests PR1 and PR2. Both fuels were fabricated with the same quantity of chromium. PR1 shows reduction of Cr content at the pellet centre whereas in PR2 the radial profile of Cr content is constant in the central part of the pellet and consistent with

the one measured after fuel fabrication. This shows that the duration of the power transient alone is too short to lead to significant oxygen redistribution.

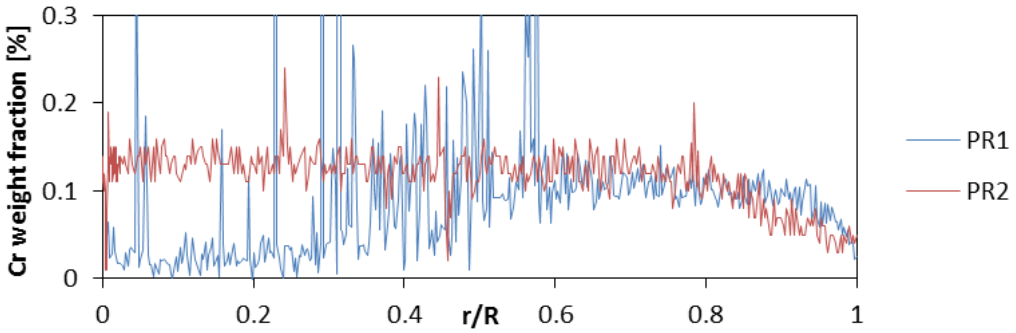



Fig. 5. EPMA measurements of chromium weight fraction in solid solution after PR1 and PR2.

The heat of transport of oxygen used in the simulation follows the one derived by Baurens [17] and is given by:

$$Q^* = -4.78 \times 10^{-4} \exp\left[7.9\left(4 - 44.63\frac{|x|}{\tau_c}\right)\right] \ [\mathrm{kJ\ mol^{-1}}]$$

where $\tau_c$ is the burnup $[\mathrm{GWd\ tU^{-1}}]$. The minimum value that this function can reach is set at -150 kJ/mol. The function is negative in the entire range of values. The oxygen chemical diffusion coefficient comes from [16] and reads:

$$D = 1.39 \times 10^{-6} e^{-75900/R_g T} [\mathrm{m^2\ s^{-1}}]$$

The flux of oxygen on the surface of the simulated fuel fragment is assumed to be null (internal corrosion of the cladding is neglected). This boundary condition ensures conservation of oxygen in the fuel pellet fragment. Oxygen migrates only in solid solution. Thus one may assume that the change of the total oxygen concentration $n_O^{tot}$ at every node (coordinates x,y,z) and during the time step (dt) is proportional to the change of the O/M ratio.

$$n^{tot}_{O(x,y,z,t+dt)} = n^{tot}_{O(x,y,z,t)} + \alpha\left(\frac{O}{M}_{(x,y,z,t+dt)} - \frac{O}{M}_{(x,y,z,t)}\right)$$

The above equation ensures conservation of $n_O^{tot}$ in the pellet since it is expressed in function of the O/M ratio which is also conserved. $\alpha$ is the factor describing the relation between $\partial n_O^{tot}$ and $\partial \frac{O}{M}$. The relation is very non-linear in the range of interest. Fig. 6 shows the total oxygen content in function of the O/M ratio at temperatures occurring in the central part of the pellet. In this simulation we assume $\alpha = 2$ since it is close to the value of the derivate $\partial n_O^{tot} / \partial \frac{O}{M}$ of the function in Fig. 6 corresponding to the oxygen content and temperatures at the centre of the pellet.

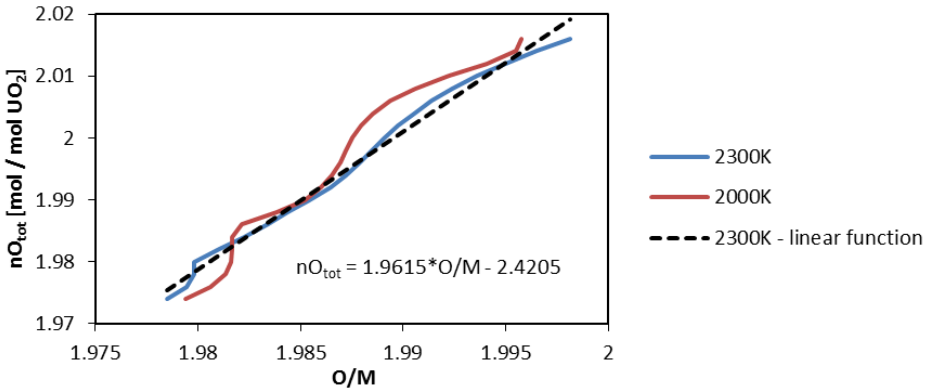



Fig. 6. Total Oxygen content $nO_{tot}$ in function of the O/M ratio at 2000 K and 2300 K. The equation describes the black line which is the linear approximation of the curve for 2300 K.

## 4. Results

According to our calculations, irradiated fuel is slightly hypostoichiometric at “t0 HP” (O/M < 2) so oxygen moves down the temperature gradient to the cold periphery. During the Holding Period, this leads to a decrease of the O/M ratio (down to ~1.975) at the centre of the pellet and an increase at the pellet periphery (up to 2). Fig. 7 shows 3D plots of the O/M ratio distribution in the simulated fuel fragment and Fig. 8 shows the radial profiles of the O/M ratio along the mid-pellet plane (top of the pellet fragment).

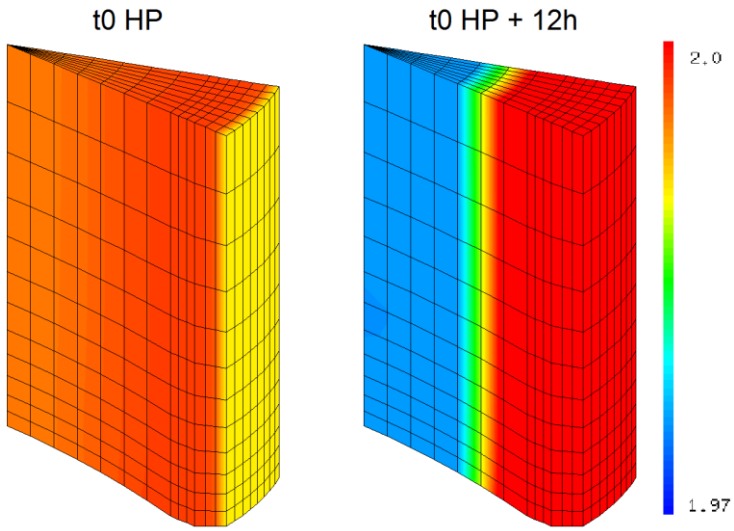



Fig. 7. O/M in the simulated fuel fragment at the beginning (left figure) and at the end (right figure) of the Holding Period. The top plane of this fragment is the mid-pellet plane and the bottom plane is the inter-pellet plane.

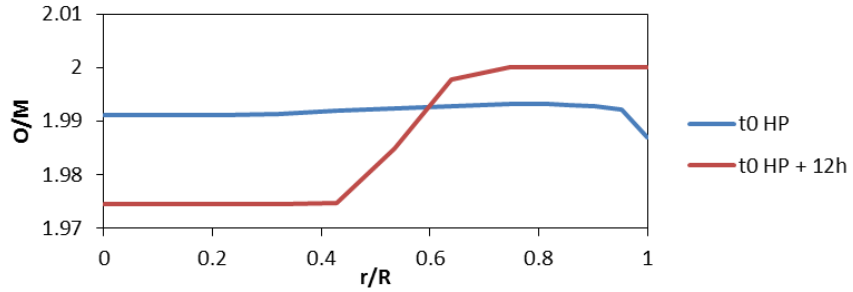



Fig. 8. O/M at “t0 HP” and “t0 HP + 12h” in function of relative radius.

Oxygen redistribution in the pellet leads to a change of the oxygen potential radial profile, as shown in Fig. 9. It is worth mentioning that radial temperature profiles at “t0 HP” and “t0 HP + 12h” are nearly the same so one may attribute oxygen potential changes to oxygen redistribution only. Initially following the temperature gradient (at t0 HP), oxygen potential at the end of the HP ranges from -450 kJ/mol at the centre to -380 kJ/mol at the periphery.

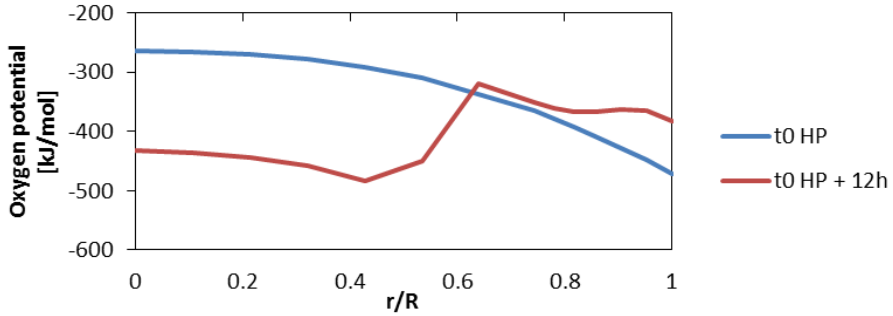



Fig. 9. Oxygen potential radial profile at mid-pellet plane at “t0 HP” and “t0 HP + 12h”.

Fig. 10 shows x-ray images of the central part of the investigated sample where one can find massive precipitation of metallic Cr (central image) and Mo (left image). They are associated with lower oxygen content (right image) which confirms their metallic form. Before the power ramp the radial profile of chromium dissolved in solid solution was constant along the radius (see Fig. 5). Thermo-diffusion of oxygen could explain the reduction of Cr and Mo and the formation of metallic precipitates at the centre of the pellet. Fig. 11 and Fig. 12 show calculated radial profiles of Cr and Mo compared to EPMA measurements. Simulation indicate a complete reduction of Mo oxides and nearly complete of Cr oxides to metallic forms in the hot part of the pellet which is consistent with post-irradiation observations. Purple curves show weight fractions measured in PR2 test which are representative of the initial non irradiated state of the fuel.

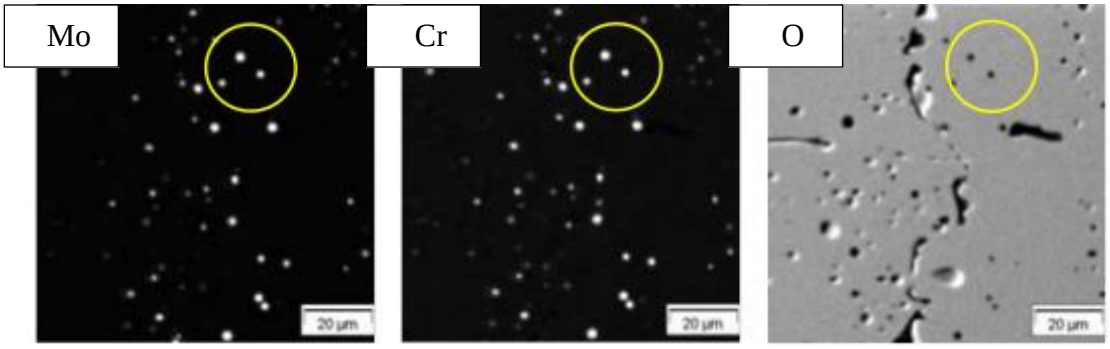



Fig. 10. X-ray images of Mo, Cr and O at the centre of the pellet [3] after PR1 test.

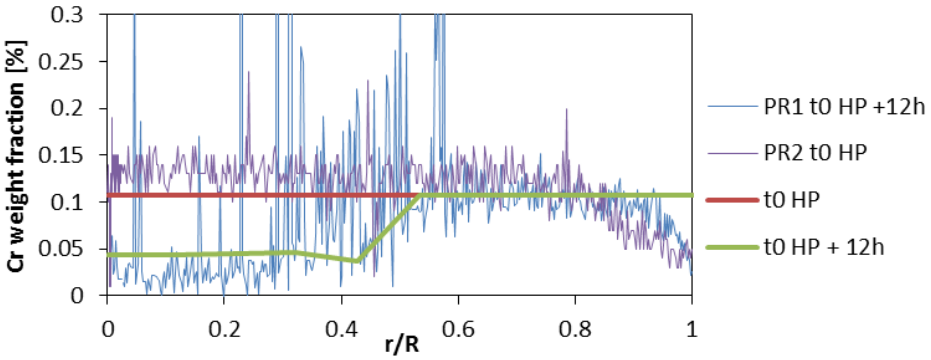



Fig. 11. Calculated Cr weight fraction evolution during the Holding Period of PR1 test compared to EPMA measurements after PR1 and PR2 tests.

According to our calculations, at the beginning of the HP ("t0 HP"), high quantities of Mo and Cs are bound together as $Cs_2MoO_{4(s,l)}$. A small fraction of Cs is in the gas phase, mostly associated to I. Reduction of $Cs_2MoO_{4(s,l)}$ at the pellet centre in consequence of oxygen redistribution liberates high quantities of caesium that form gaseous compounds (mainly $Cs_{(g)}$ and $Cs_{2(g)}$) that can then be released from the pellet during the holding period. Fig. 13 shows the calculated concentrations of Cs in gaseous and condensed forms at the beginning and at the end of the Holding Period. Total quantity of Cs in the central part of the pellet after the ramp is lower due to gas release but it is not as low as EPMA measurements that show nearly complete release in the central part.

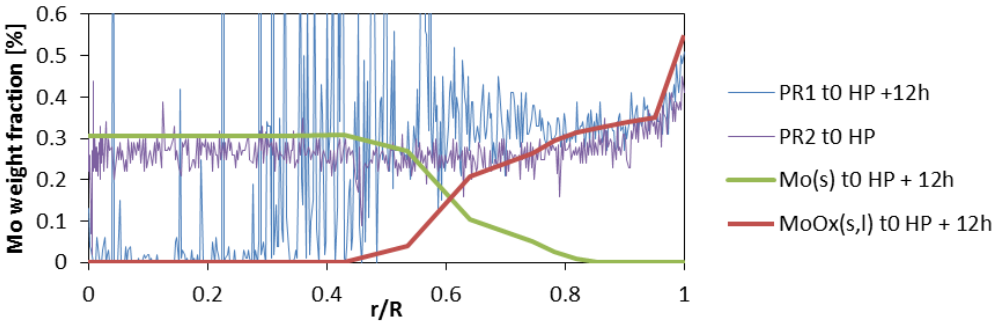



Fig. 12. Calculated molybdenum oxides $MoO_{x(s,l)}$ and metallic molybdenum $Mo_{(s)}$ weight fraction evolution during the Holding Period of PR1 tests compared to EPMA measurements after PR1 and PR2 tests. PR2 rodlet has a slightly lower burnup than PR1 rodlet so the Mo weight fraction is lower on average.

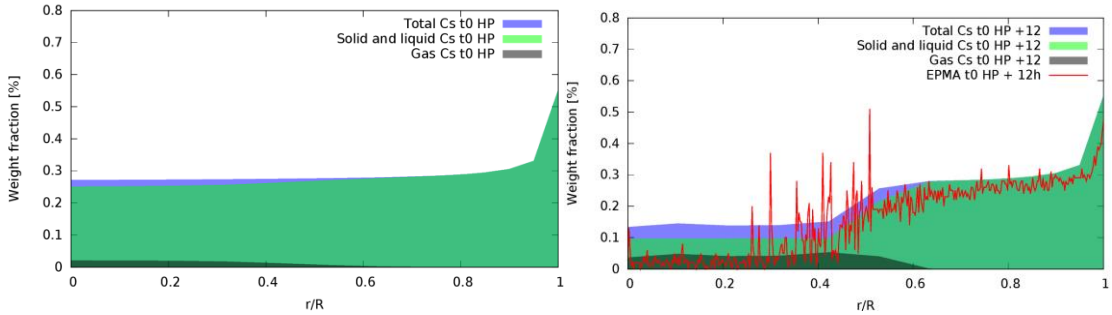



Fig. 13. Calculated speciation of caesium at “t0 HP” and “t0 HP + 12h” along the inter-pellet plane compared to EPMA measurements after PR1 test.

The rest of liberated Cs reacts with Te to form $Cs_2Te_{(s)}$. Reduction of caesium molybdate is important from the point of view of PCI. At the beginning of the Holding Period, part of the total iodine is available in gas form as $I_{2(g)}$, $I_{(g)}$ and $TeI_{2(g)}$. When released from the fuel pellet, all three species can potentially react with Zr-cladding to form $ZrI_{4(g)}$ and hence induced Iodine Stress Corrosion Cracking (I-SCC). When gaseous $Cs_{(g)}$ or $Cs_{2(g)}$ species are released from the fuel pellet, they are likely to interact with the iodide species $I_{2(g)}$, $I_{(g)}$ and $TeI_{2(g)}$ already in the rodlet free volume to form the thermodynamically very stable $CsI_{(g)}$, which is known to be quite unreactive chemically towards Zr [18]. Fig. 14 shows the differences in speciation of gaseous iodine between the beginning and the end of the Holding Period. Around 80% of the initial iodine inventory is released at the pellet centre.

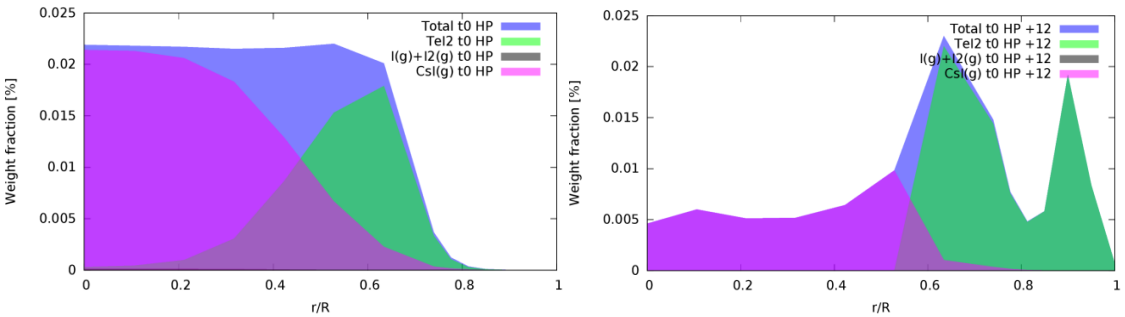



Fig. 14. Speciation of gaseous iodine at “t0 HP” and “t0 HP + 12h” along the inter-pellet plane.

Fig. 15 shows 3D results of Xe, Cs and I release (in % of the initial inventory) at the end of the holding period. One may notice much higher release near the dish. It is related to lower hydrostatic pressure. Fig. 16 shows Xe weight fractions at “t0 HP” and “t0 HP + 12h” along the inter-pellet plane and the comparison to EPMA and SIMS measurements. At the end of the HP, around 14% of the total Xe content of the pellet fragment has been released.

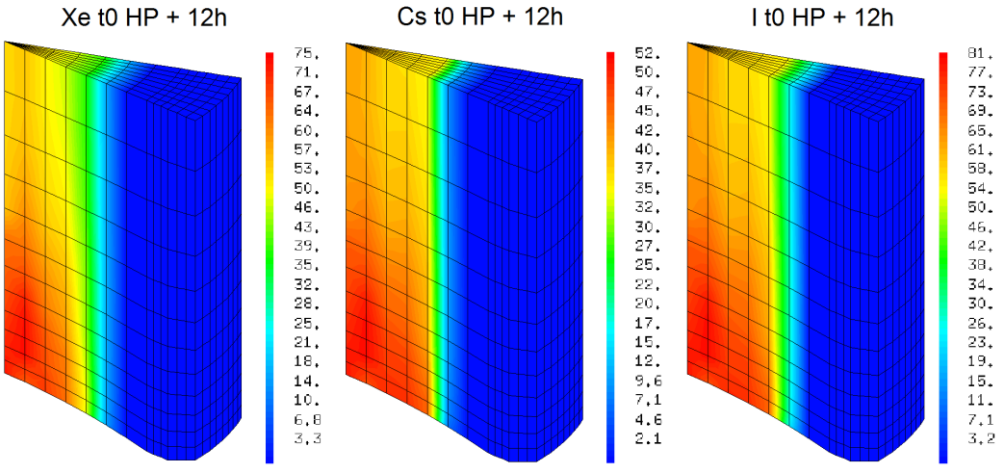



Fig. 15. Release of Xe, Cs and I at “t0 HP + 12h”. Units - % of initial inventory.

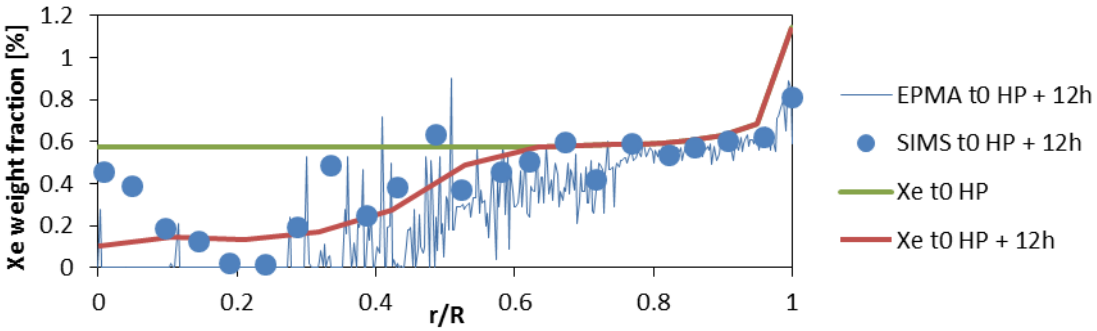



Fig. 16. Total (dissolved within grains, in intra- and inter-granular bubbles and in inter-granular pores) Xe weight fraction at the beginning and the end of the holding period compared to EPMA and SIMS measurements.

Fig. 17 shows release of Cs, I and Xe in function of time (solid lines). Results compared to the same simulation without oxygen redistribution show higher release of iodine and much lower release of caesium (dashed lines). Oxygen redistribution does not have impact on calculated Xe release but is known to modify diffusion coefficient of rare gases especially during oxidation of fuel pellets [19].

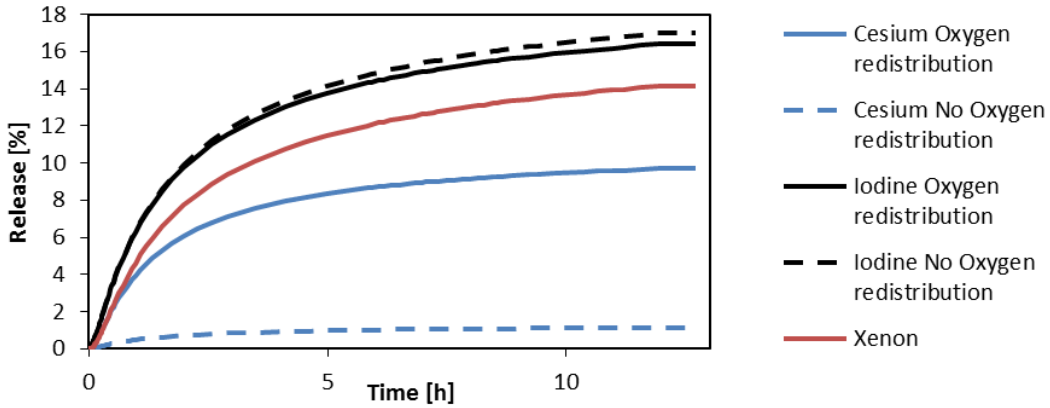



Fig. 17. Release of Cs, I and Xe in function of time. Solid lines – simulation with oxygen redistribution, dashed lines – simulation without oxygen redistribution. The graph starts at “t0”.

## 5. Conclusion

The main purpose of this paper was to show the impact of oxygen thermo-diffusion on the chemical state of FPs. In this aim, a complex thermo-mechanical-chemical 3D simulation of a power ramp has been carried out with the fuel performance code ALCYONE which includes

the thermochemical solver ANGE. Calculated radial profiles of Cr and Mo after the power ramp match the experimental measurements. The reduction of Cr and Mo oxides into metallic precipitates is recovered in the simulation thanks to oxygen redistribution. The consecutive reduction of caesium molybdate leads to the formation of high quantities of free gaseous caesium that can then be released from the fuel pellet core, in agreement with experimental measurements. Decomposition of caesium molybdate is expected to be of some importance for PCI since iodide gas species released from the fuel in the free volume of the rodlets can form unreactive caesium iodide and hence reduce the potential for Iodine Stress Corrosion Cracking of Zr cladding. One of the benefits of Cr dopants could be related to the solubility of chromium that modifies the magnitude of oxygen redistribution during a power ramp.

## 6. Acknowledgements

The authors would like to thank FRAMATOME and EDF for their financial support and fruitful discussions.

## 7. References

[1] B. Baurens, J. Sercombe, C. Riglet-Martial et al., *J. Nucl. Mat.*, 452, pp. 578-594, 2014.

[2] C. Nonon et al., "PCI behaviour of chromium oxide-doped fuel," *Pellet-clad interaction in water reactor fuels, OECD-NEA,* Aix-en-Provence, France, 2004.

[3] C. Riglet-Martial, J. Sercombe et al., *J. Nucl. Mat.*, 480, pp. 32-39, 2016.

[4] V. Marelle, "Validation of PLEIADES/ALCYONE 2.0 fuel performance code," in *Water Reactor Fuel Performance Meeting*, Jeju Island, Korea, 2017.

[5] Cast3M, *http://www-cast3m.cea.fr/, [Online]*.

[6] J.-M. Vidal, *Waste Management, Phoenix, Arizona, USA*, 2012.

[7] P. Garcia, *Water reactor fuel element modelling at high burnup and its Experimental Support*, Windermere, UK, 1994.

[8] T. M. Besmann and T. B. Lindemer, *J. Nucl. Mat.*, 130, pp. 489-504, 1985.

[9] T. B. Lindemer and T. M. Besmann, *J. Nucl. Mat.*, 130, pp. 473-488, 1985.

[10] T. B. Lindemer and J. Brynestad, *J. Am. Ceram. Soc.*, 69, pp. 867-876, 1986.

[11] J. Dumas, *PhD thesis*, 1995, Institut National Polytechnique, Grenoble, France.

[12] T. Fujino, *J. Nucl. Mat.*, 154, pp. 14-24, 1988.

[13] C. Riglet-Matial, *J. Nucl. Mat.*, 447, pp. 63-72, 2014.

[14] G. Jomard et al., "CARACAS: an industrial model for description of fission gas behavior in LWR-UO2 fuel," *WRFPM 2014, Sendai, Japan*, 2014.

[15] C. Sari et G. Schumacher, *J. Nucl. Mat.*, 61, pp. 192-202, 1976.

[16] K. Lassmann, *J. Nucl. Mat.*, 150, pp. 10-16, 1987.

[17] B. Baurens, "Couplages thermo-chimie-mécaniques dans l'UO2 – Application à l'interaction pastille-gaine," *Phd thesis, Université Aix-Marseille*, 2014.

[18] D. Cubicciotti, "Chemical aspects of iodine-induced stress corrosion cracking of zircaloys," in *Zirconium in the Nuclear Industry*, Boston, USA, 1982.

[19] K. Une, *J. Nucl. Mat.*, 150, pp. 93-99, 1987.